Preprint typeset in JINST style - HYPER VERSION

Luminescence quenching of the triplet excimer state by air traces in gaseous argon

C. Amsler[a]*, V. Boccone[a], A. Büchler[a], R. Chandrasekharan[b], C. Regenfus[a] and J. Rochet[a]

[a] *Physik-Institut der Universität Zürich, Winterthurerstrasse 190, CH-8057 Zürich, Switzerland*
[b] *Institute for Particle Physics, ETH-Zürich, CH–8093 Zürich, Switzerland*
E-mail: Claude.Amsler@cern.ch

ABSTRACT: The influence of air contamination on the VUV scintillation yield in gaseous argon at atmospheric pressure is investigated. We determine with a radioactive α-source the photon yield for various partial air pressures and different reflectors and wavelength shifters. We find that the time constant of the slow scintillation component depends on gas purity and is a good indicator for the total VUV light yield, while the fast component is not affected. This dependence is attributed to impurities destroying the long-lived triplet argon excimer state. The population ratio between the slow and the fast decaying excimer states is determined for α-particles to be 5.5 ± 0.6 in argon gas at 1100 mbar and room temperature. The measured decay time constant of the slow component is 3.140 ± 0.067 μs at a partial air pressure of 2×10^{-6} mbar.

KEYWORDS: Argon scintillation, VUV detection.

*Corresponding author.

Contents

1. Introduction

Noble liquids such as argon (or xenon) can act as targets for WIMPs (Weak Interacting Massive Particles), the most popular candidates for dark matter in the universe. These elements have high scintillation yields and are also suitable for charge detection because of their relatively low ionization potentials. Both ionization and scintillation light can be detected [1, 2]. Argon (^{40}Ar) is cheap compared to xenon and is therefore competitive for large volumes, in spite of its contamination by the ^{39}Ar β-emitter. Here we present measurements on gaseous argon done while developing the scintillation light readout of a 1 ton liquid argon TPC to search for dark matter (ArDM [2]).

The light yield and the mechanism for the luminescence of noble gases and liquids are comparable to those of alkali halide crystals [3, 4] and are described in the literature for dense gases [5, 6] and liquids [7, 8, 9, 10]. Fundamental to the scintillation process is the formation of excited dimers (excimers) which decay radiatively to the unbound ground state of two argon atoms. Figure 1 shows schematically the two mechanisms leading to light emission in argon, excitation and ionization. Excitation leads through collisions with neighbouring atoms to neutral excimers Ar_2^* which decay radiatively into two argon atoms. Ionization leads to the formation of charged excimers which are neutralized by thermalized electrons (recombination luminescence). Both processes are strongly pressure and density dependent. Recombination is also sensitive to external electric fields. For gaseous argon at room temperature and normal pressure, at which we operate here, excitation dominates [11, 12], while recombination luminescence becomes important at high pressures or in liquid.

In liquid argon the population ratio of the fast to slow-decaying states depends on the type of projectile, e.g. electron, α-particle or fission fragment. The population ratio of the fast to slow decaying states increases with stopping power and is 0.3, 1.3 and 3 for electrons, α-particles and fission fragments, respectively (for a compilation see ref. [9]). However, the decay times are not affected. The measured time constants scatter in the range between 4 and 7 ns for the fast component and between 1.0 and 1.7 μs for the slow component. The large difference in the two time constants is unique for argon among noble gases and can be used to suppress background in

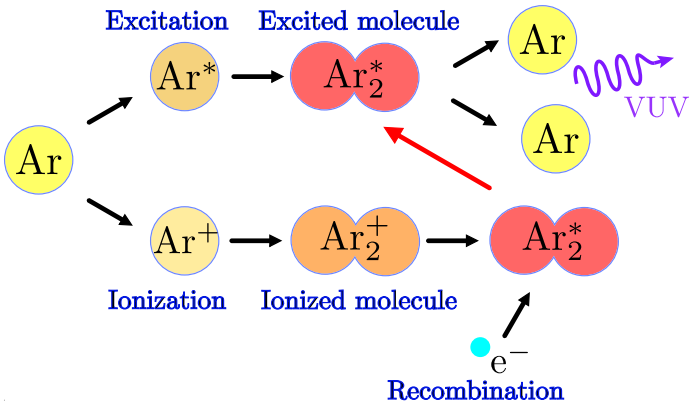

Figure 1. *The two mechanisms leading to the emission of 128 nm photons (adapted from ref. [6]).*

WIMP searches, since WIMP-interactions lead to heavily ionizing recoil nuclei and hence to a high population of the fast decaying states.

Of special interest to this work is the long lived component which is attributed to the excitation of the lowest spin-triplet excimer state with a mean life of 3.2 ± 0.3 μs, which is pressure independent in gas between 1 and 30 atm [5]. This state decays radiatively by emitting VUV photons in a $\approx$10 nm band around 128 nm [13, 14] (second excimer continuum). These photons are not absorbed by atomic argon and can therefore be detected. Light at higher wavelengths is also produced from transitions between highly excited argon atomic states [14, 15, 16].

In this paper we present evidence for the (non-radiative) destruction of the triplet state in gaseous argon by traces of air [17, 18]. The population of the triplet states decreases exponentially with a shorter decay time than measured with clean argon gas. The reduced light yield is presumably due to collisional destruction of the long-lived triplet state by impurities such as water molecules. A similar effect is observed in liquid argon [19].

2. Experimental setup

The apparatus consists of a 6 liter cylindrical vessel, 150 mm in inner diameter (with no internal electrical field), equipped with a variety of service connections, e.g. to a quadrupole mass spectrometer (fig. 2). Pumping is carried out by a dry primary pump and a 60 liter/s turbo pump. Without baking a typical vacuum of 10^{-5} mbar is reached within 24 h. The residual gas is mainly composed of water vapour. The surrounding dewar is used for measurements with liquid argon. The present measurements are performed with a Hamamatsu R580 photomultiplier (PMT), 38 mm diameter with bialkali photocathode. A reflecting collar (MgF_2 coated aluminium) concentrates the light on the photocathode. A 40 Bq ^{210}Pb source (half life 21.4 yrs [20]), emitting 5.3 MeV α-particles and up to 1.2 MeV electrons (^{210}Pb $\rightarrow$ ^{210}Bi $\rightarrow$ ^{210}Po $\rightarrow$^{206}Pb), is mounted in the center of the vessel, about 6 cm below the photomultiplier. The range of the α-particles is roughly 4.5 cm in argon gas at NTP (density 1.78 g/l). Hence α-particles are fully absorbed while electrons from the source are not fully contained. The average number of 128 nm photons in pure argon gas is estimated to be 78 000, assuming an energy expenditure of about 68 eV/photon [21].

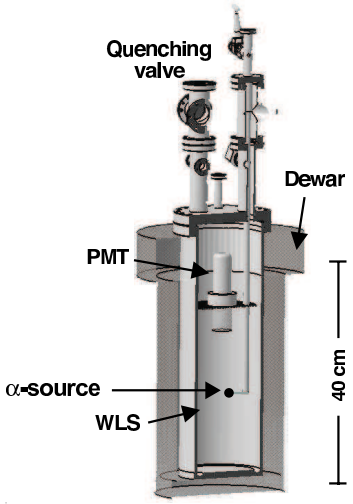

Figure 2. *Vessel for gaseous and liquid argon measurements.*

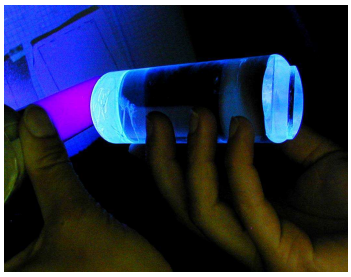

Figure 3. *Trapping of the shifted blue light in a plexiglas cylinder.*

Argon gas is taken from 50 liter cylinders of class Ar 60 (impurities ≤ 1.3 ppm). An oxisorb (CuO) filter and a hydrosorb cartridge (molecular sieve) are used during filling. The VUV scintillation light is converted into blue light with tetraphenyl-butadiene (TPB) as a wavelength shifter (WLS), sprayed on Tetratex or 3M (ESR vikuiti) foils. The emission spectrum of TPB reaches its maximum value at 422 nm [22] and matches the response of bialkali photocathodes (300 – 600 nm). The typical time constant of TPB is 2 ns [23] and the time constant of the PMT 4.5 ns. The WLS material is dissolved in chloroform and sprayed (or evaporated) on reflecting foils covering the internal wall of the vessel. To improve on the overall light collection yield the glass window of the phototubes can also be coated with WLS. The coating is performed with TPB imbedded in a clear polymer matrix such as polystyrene or paraloid. Figure 3 demonstrates trapping of the shifted blue light in a plexiglas cylinder, one end of which has been covered with TPB/polystyrene.

The R580 PMT is operated at –1350 V bias voltage yielding a gain of roughly 10^6. Its signal is amplified by a factor of 10 in a fast NIM amplifier (CAEN N979) and fed to the 8 bit FADC of a LeCroy WP7100 digital oscilloscope terminated with 50Ω. The signal is sampled at a rate of 1 GHz and, for each event, 20 000 samples covering 20 μs are recorded and stored in compressed MatLab file format to hard disk, in packages of about 1000 events.

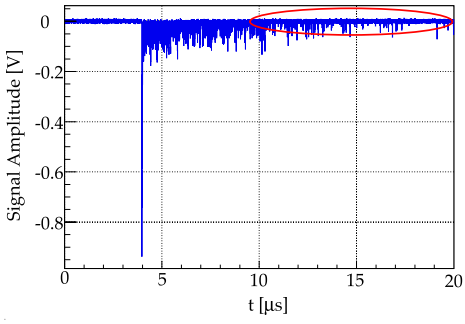

Figure 4. *Sampling of an α-event in gaseous argon. The ellipse shows the region dominated by single photon pulses.*

3. Measurement of the decay spectrum

The measurements presented in this paper were collected at an argon pressure of 1100 mbar and at room temperature, except for the data at the partial air pressure of 2×10^{-6} mbar, which were taken slightly below the water freezing point ($\sim$–20°C). The latter constitute our cleanest argon sample. A typical event generated by the α-source at 2×10^{-6} mbar is shown in fig. 4. The large prompt pulse is mainly due to the fast scintillation component, the slowly decaying amplitude to the slow component, and the pulse at large sampling times (ellipse) to late arriving single photons. The event trigger in the oscilloscope is set on the analogue signal height in the range of -20 to -2000 mV, depending on the data set to be taken. The typical height of a single photoelectron pulse after the $10\times$ amplification amounts to roughly -35 mV.

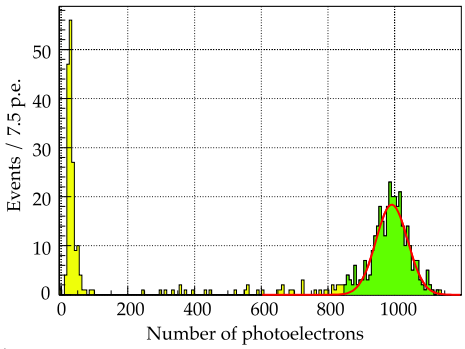

Figure 5. *Pulse height distribution of 321 α-decays at a partial air pressure of 2×10^{-6} mbar.*

Before integration the pedestal is determined event-wise by averaging over the first couple of thousand data points before the trigger. The total number of photoelectrons is then calculated by dividing the integrated signal (charge) by the average single photon charge, which we find from the integrated distribution of dark counts. Single photon events from the signal tails (ellipse in fig. 4) were used for a cross-check only since they are affected by pile-up. Figure 5 shows a typical integrated pulse height distribution for a sample of 528 events at a partial air pressure of 2×10^{-6} mbar. The peak (321 events) is due to α-particles. An integrated charge of 1 nVs over 50Ω corresponds to 6.8 ± 0.2 photoelectrons (p.e.).

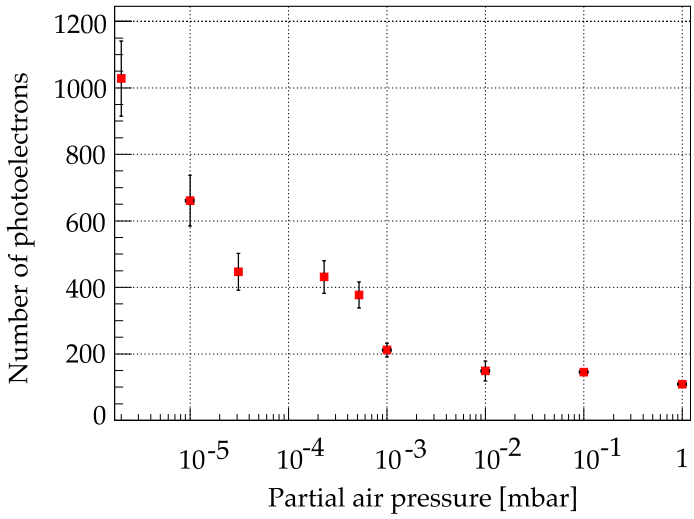

Figure 6. *Light yield of α-particles in argon gas vs. partial air pressure at room temperature. The data at 2×10^{-6} mbar were taken below the water freezing point ($\sim$–20°C).*

We now discuss the light yield as a function of gas purity which depends on the vacuum pressure in the vessel before letting argon in. Measurements were started by evacuating the vessel down to pressures around 10^{-3} mbar. Air was then introduced up to atmospheric pressure and pumped out until the desired pressure was achieved. Gaseous argon was then introduced until a pressure of 1100 mbar was reached. Figure 6 shows the number of photoelectrons as a function of partial air pressure. The number of photoelectrons clearly depends on the purity of the argon and still rises below 10^{-5} mbar at which pressure the dominating contribution is outgassing from the vessel. The minimum pressure that could be achieved in the vessel was around $\sim 10^{-6}$ mbar by cooling with cold nitrogen.

Next, we add the sampled pulse distributions from many α-decays with total charge within $\pm 3\sigma$ from the peak value (see fig. 5), and determine the average charge and its error for each 1 ns bin. Figure 7a shows a semilogarithmic representation of the average amplitude vs. time for the 321 α-events above, taken at 2×10^{-6} mbar. The dark (black) area represents the data points, the grey (green) area the r.m.s errors. Figure 7b shows a zoom on the first 400 ns

The red line shows the fit to the data with two exponentials to model the fast and slow decays, convoluted with a gaussian G to describe the experimental resolution. A step function H and a free parameter are used to fit the event time t_0. Hence the model function has 6 free parameters and is given by

$$\begin{aligned} f &= G(t - t_0, \sigma) \\ &\otimes H(t - t_0) \left[\frac{A}{\tau_1} e^{-\frac{t-t_0}{\tau_1}} + \frac{B}{\tau_2} e^{-\frac{t-t_0}{\tau_2}} \right], \end{aligned} \tag{3.1}$$

where $H(t - t_0) = 1$ for $t > t_0$ and 0 for $t < t_0$. The parameters τ_1 and τ_2 are the time constants of the fast and slow-decaying states. The parameters A and B are proportional to the total number

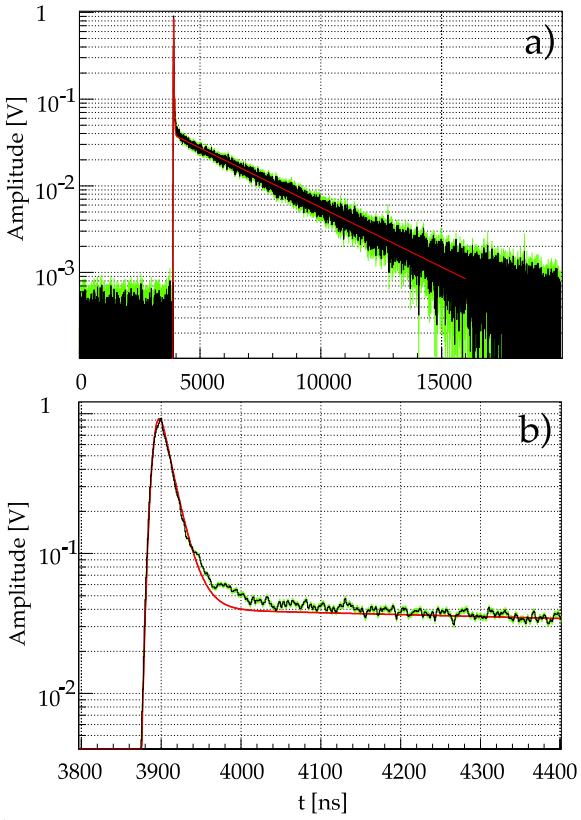

Figure 7. *a) Average signal from α-decays in clean argon gas; b) zoom into the first 400 ns (see text).*

of photoelectrons detected from the two components. In the absence of non-radiative de-excitation processes, they describe the populations of the two initial states.

Both components are clearly visible in fig. 7. The fit is in good agreement with data, except in the intermediate region ($t - t_0 \sim$150 ns). The slight excess of data in this region (probably due to an additional process) does not affect our results on the fast and slow time constants. We have fitted a third exponential ($\tau_3 \sim$100 ns) and also performed fits without the 3.94 – 4.20 μs region. We use these fits to assess the (dominating) systematical errors. For the data shown in fig. 7 we find τ_1 = 14.7 $\pm$ 2.5 ns, τ_2 = 3140 $\pm$ 67 ns and a ratio $R \equiv B/A$ = 5.5 $\pm$ 0.6. The fitted r.m.s. resolution σ of 5.6 ns is consistent with the time constant of the PMT (4.5 ns), including the transit time of α-particles ($\sim$4ns).

The time distributions for various partial air pressures and the corresponding fits using eqn. (3.1) are shown in fig. 8. The time constants τ_1, τ_2 and the amplitudes A and B are given in Table 1. The time constant of the fast component and its photoelectron yield remain constant within errors. From Table 1 the average value for τ_1 is 11.3 $\pm$ 2.8 ns and is compatible with values obtained earlier [14]. In contrast, the time constant τ_2 of the slow component and its photoelectron yield clearly increase with gas purity. Our result for τ_2 is in good agreement with a previous measurement in dense gases, 3.2 $\pm$ 0.3 μs [5], but is more precise.

For each measurement, two batches of data were taken consecutively, the second about 10 – 15 min later than the first. The number of photoelectrons decreased slightly between the first and the

Table 1. *Time constants τ_1 and τ_2 for various residual air pressures at room temperature. A and B are proportional to the total number of photoelectrons from each component.*

p [mbar]	τ_1 [ns]	A [nVs]	τ_2 [ns]	B [nVs]
1	$\simeq$10	9.5 (0.2)	114 (9)	6.5 (0.4)
10^{-1}	$\simeq$10	12.7 (0.3)	198 (14)	8.7 (0.4)
10^{-2}	11.0 (0.6)	12.8 (0.3)	240 (57)	9.1 (1.8)
10^{-3}	11.9 (1.7)	14.0 (0.8)	520 (59)	17.1 (1.2)
5.2×10^{-4}	12.7 (2.8)	15.6 (1.5)	1341 (44)	39.9 (0.8)
2.3×10^{-4}	12.8 (2.8)	14.8 (1.6)	1788 (43)	48.6 (0.7)
3×10^{-5}	13.2 (2.9)	15.2 (1.8)	1817 (44)	50.5 (0.6)
10^{-5}	12.6 (2.8)	14.5 (1.6)	2992 (33)	82.6 (0.4)

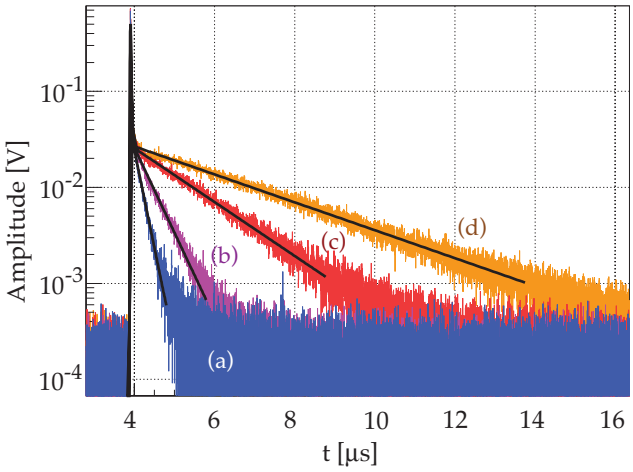

Figure 8. *Average signal from α-decays for various residual air pressures: 10^{-2} mbar (a), 10^{-3} mbar (b), 2.3×10^{-4} mbar (c) and 10^{-5} mbar (d).*

second batches. However, with cooling, the second batch contained slightly more photoelectrons. This suggests in the first case outgassing of water molecules and, in the second case, freezing water on the walls of the vessel. Nitrogen contamination, on the other hand, does not lead to a strong suppression of VUV light [13]. Hence the partial pressure of water might be responsible for the non-radiative destruction of the triplet states.

We have also investigated the nature of the slow and fast components by using two PMTs installed, one at the bottom, the other at the top of a gas vessel. One of the PMT photocathodes was covered with a 5 mm thick quartz plate. With the quartz absorber one observes a very strong suppression of the slow component (fig. 9) while the fast component is not affected. The measured absorption spectrum in fig. 9 right shows that light with a wavelength below 160 nm is strongly absorbed. This indicates that the slow component consists dominantly of VUV light (second con-

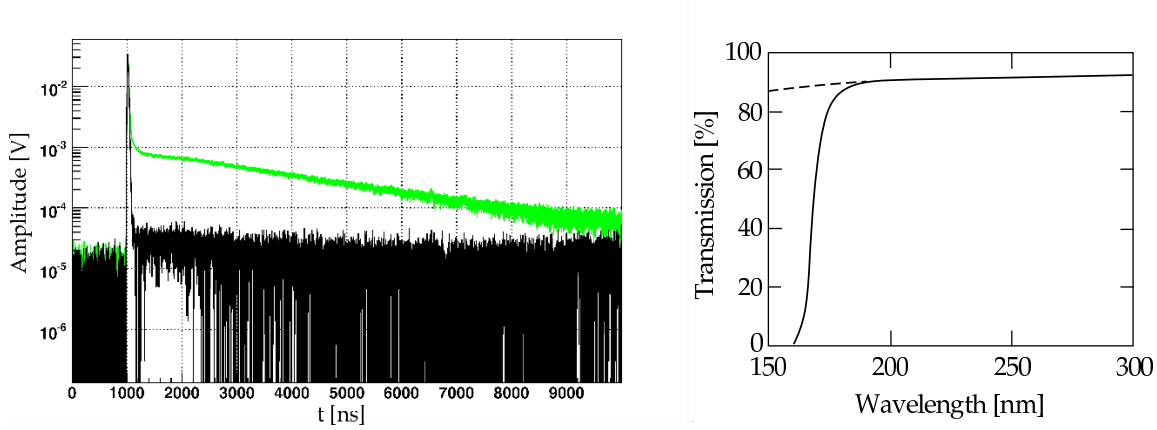

Figure 9. *Left: average signal from α-decays at 1200 mb in clean gas (top distribution). The bottom time distribution was obtained by inserting a quartz plate in front of the PMT photocathode. Right: absorption spectrum of the quartz plate as a function of wavelength (full curve). The dashed line shows the transmission efficiency without absorption, but taking into account the Fresnel surface reflection from the quartz plate.*

tinuum around 128 nm), while the fast component is mainly composed of UV light with wavelength from the third continuum above 160 nm [14].

4. Slow to fast population ratio

Since τ_1 and A do not depend on gas purity, we can determine the ratio of slow to fast populations by measuring the light yield as a function of τ_2 and extrapolating to pure argon gas. Indeed, the light yields being proportional to A and B, the population B_1 of the long-lived state is given by $B = B_1\Gamma_\gamma\tau_2$, where Γ_γ is the radiative width, while the population of the short-lived state is proportional to A. The slow to fast population ratio is then equal to the ratio $R = B/A$ for $\Gamma_\gamma = 1/\tau_2$, i.e. for pure argon gas. Figure 10 shows the total number of photoelectrons as a function of τ_2 for the various gas purities given in Table 1. Extrapolating τ_2 to τ_2^m = 3.2 μs obtained earlier with gas of highest purity [5] we find $R = 5.5 \pm 0.6$ for 5.3 MeV α-particles in clean argon gas at 1100 mbar and room temperature. To our knowledge this ratio R of the slow (VUV) to the fast (UV) components has not been measured before.

We have also performed measurements of the light yield for a series of WLS configurations. These data provide a cross-check for the measurements presented above. The PMT photocathode was either coated with TBP/polystyrene or sprayed with TPB, and the reflecting foil (3M or Tetratex) sprayed with TPB of various thicknesses. Figure 11 shows the various measurements. As in fig. 10 we extrapolate the data points to the expected decay time of τ_2^m = 3.2 μs for the second component in pure argon. However, we now require the straight lines to intersect the τ_2-axis at the common fitted point $\tau_2^0 = -485^{+100}_{-150}$ ns, where $A + B = 0$. The simple proportionality $R = B_1/A = \tau_2^m/\tau_2^0$ leads to the population ratio $R = 6.6^{+2.1}_{-1.5}$. This number agrees with our determination above, but is much less precise due to the large lever arms in the extrapolation to τ_2^0.

Summarizing, we have measured the light yield in gaseous argon for various residual air pressures. For the slow component of the luminescence at 128 nm we observe a strong dependence on residual air pressure. This effect is attributed to contaminating water vapour. The longest time

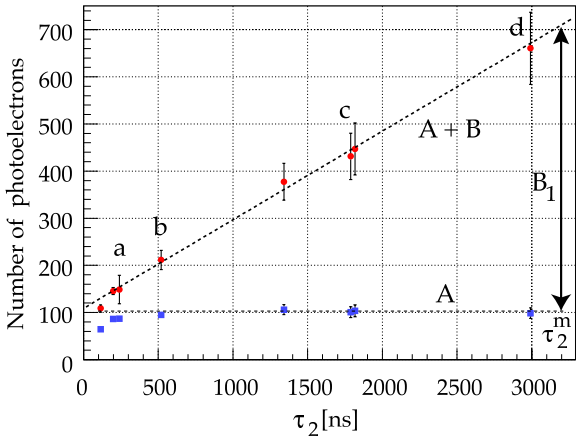

Figure 10. *Total number of photoelectrons as a function of τ_2. The upper dashed line gives the fitted total light yield ($A+B$) from both components, the bottom dashed line the fast contribution (A). The labels a – d refer to the data shown in fig. 8.*

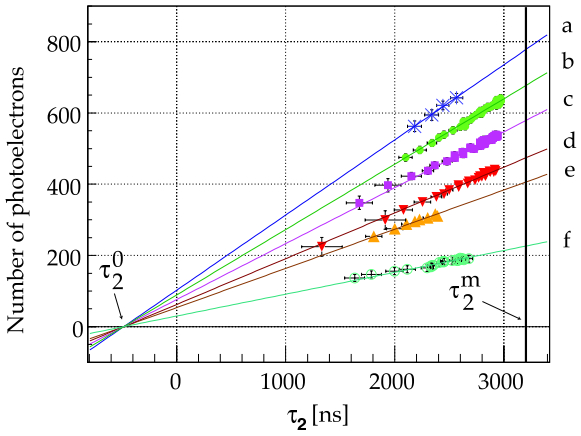

Figure 11. *Light yield of α-particles in argon gas for different WLS coating and application techniques: a) coated PMT and sprayed 3M-foil; b) sprayed PMT and 3M-foil; c) sprayed 3M-foil ; d) sprayed PMT ($\sim$0.4 mg/cm^2) and Tetratex; e) sprayed PMT ($<$0.1 mg/cm^2) and Tetratex; f) sprayed PMT and MgF_2 coated mirror foil.*

constant is obtained from purest argon (3140 $\pm$ 67 ns). The population ratio between the slow and the fast decaying states is measured for α-particles to be R = 5.5 $\pm$ 0.6 in pure argon gas at 1100 mbar and room temperature.

Acknowledgments

We thank Hugo Cabrera and Andreas Knecht for their contributions in developing the reflector foils and wavelength shifters. We thank A. Braem and C. David for the measurement of the quartz transmission spectrum, Mario Thomann for the measurement of the decay spectra with the quartz absorber, Marco Laffranchi for preparing the radioactive source, and the ArDM collaboration for valuable discussions and comments. This work was supported by a grant from the Swiss National

Science Foundation.

References

[1] N. Ferrari (WARP Collaboration), *WARP: a double phase argon programme for dark matter detection*, J. Phys. Conf. Ser. **39** (2006) 111

[2] A. Rubbia (ArDM Collaboration), *ArDM: a ton-scale liquid Argon experiment for direct detection of Dark Matter in the Universe*, J. Phys. Conf. Ser. **39** (2006) 129

[3] J. Jortner et al., *Localized Excitons in Condensed Ne, Ar, Kr and Xe*, J. Chem. Phys. **42** (1965) 4250

[4] O. Cheshnovsky and B. Raz, *Temperature Dependence of Rare Gas Molecular Emission in the Vacuum Ultraviolet*, Chem. Phys. Lett. **15** (1972) 475

[5] J. W. Keto, R. E. Gleason Jr., and G. K. Walters, *Production Mechanisms and Radiative Lifetimes of Argon and Xenon Molecules Emitting in the Ultraviolet*, Phys. Rev. Lett. **33** (1974) 1365

[6] M. Suzuki, J. Ruan(Gen) and S. Kubota, *Time dependence of the recombination luminescence from high-pressure argon, krypton and xenon excited by alpha particles*, Nucl. Instr. Meth. **192** (1982) 565

[7] S. Kubota et al., *Recombination luminescence in liquid argon and in liquid xenon*, Phys. Rev. **B 17** (1978) 2762

[8] S. Kubota, M. Hishida and J. Ruan(Gen), *Evidence for a triplet state of the self-trapped exciton states in liquid argon, krypton and xenon*, J. Phys. **C 11** (1978) 2645

[9] A. Hitachi et al., *Effect of ionization density on the time dependence of luminescence from liquid argon and xenon*, Phys. Rev. **B 27** (1983) 5279

[10] T. Doke, K. Masuda and E. Shibamura, *Estimation of absolute photon yields in liquid argon and xenon for relativistic (1 MeV) electrons*, Nucl. Instr. Meth. in Phys. Res. **A 291** (1990) 617

[11] M. Suzuki, *Recombination luminescence from ionization tracks produced by alpha particles in high pressure argon, krypton and xenon gases*, Nucl. Instr. Meth. **A 215** (1983) 345

[12] M. J. Carvalho and G. Klein, *Alpha-particle induced scintillation in dense gaseous argon: emission spectra and temporal behaviour of its ionic component*, Nucl. Instr. and Meth. **178** (1980) 469

[13] T. Takakashi, S. Himi, M. Suzuki, J. Ruan(Gen) and S. Kubota, *Emission spectra from Ar–Xe, Ar–Kr, Ar–N_2, Ar–CH_4, Ar–CO_2 and Xe–N_2 gas scintillation proportional counters*, Nucl. Instr. Meth. **A 205** (1983) 591

[14] W. Krötz, A. Ulrich, B. Busch, G. Ribitzki, and J. Wieser, *Third excimer continuum of argon excited by a heavy-ion beam*, Phys. Rev. **A 43** (1991) 6089

[15] K. Aho, P. Lindblom, T. Olsson, O. Solin, *Pressure-dependent decay of the $3p^5 4p$ configuration in argon excited by alpha-particle and protons*, J. Phys. B: At. Mol. Opt. Phys. **31** (1998) 4191 (and references therein)

[16] P. Lindblom, O. Solin, *Atomic near-infrared noble gas scintillations I, Optical spectra*, Nucl. Instr. Meth. in Phys. Res. **A 268** (1988) 204

[17] A. Büchler, Bachelor Thesis, University of Zürich, 2006 http://unizh.web.cern.ch/unizh/nouveau/nouveausite/Publications/Articles/bachelorAngela.pdf

[18] C. Regenfus, *Detection of VUV scintillation light in one ton of liquid argon*, Proc. IDM2006 Conf., World Scientific (in print)

[19] C. Amsler et al., in preparation

[20] W.R. Eckelmann, W.S. Broecker, and J.L. Kulp, *Half-Life of Pb^{210}*, Phys. Rev. **118** (1960) 698

[21] R. Chandrasekharan, M. Messina, A. Rubbia, *Detection of noble gas scintillation light with large area avalanche photodiodes (LAAPDs)*, Nucl. Instr. Meth. in Phys. Res. **A 546** (2005) 426

[22] Starna Brand, *Reference Materials for Molecular Fluorescence Spectroscopy*, http://www.optiglass.com

[23] J. Huang et al., *Study of poly(methyl methacrylate) thin films doped with laser dyes*, Journal of Luminescence **81** (1999) 285